Design and Synthesis of Parallel-Connected Dielectric Filter Using Chain-Function Polynomial

Francis E. CHINDA [1], Sovuthy CHEAB [2], Socheatra SOEUNG [1]

[1] Dept. of Electrical and Electronic, Universiti Teknologi PETRONAS, Bandar Seri Iskandar, Perak 32610, Malaysia
[2] FILPAL (M) Snd Bhd, Bayan Lepas, Penang 11900, Malaysia

Emmanuel_19000968@utp.edu.my, vuthy@filpal.com, socheatra.s@utp.edu.my

Submitted August 8, 2022 / Accepted October 26, 2022 / Online first January 9, 2023

Abstract. *Design and synthesis of parallel connected dielectric filters using chained function polynomials are presented in this paper. This filter will offer reduced sensitivity to fabrication tolerance while preserving its return loss response within the desired bandwidth in comparison to traditional Chebyshev filters. A novel transfer function FN according to chained is derived for fourth and sixth-order filters and the synthesis technique is presented. To demonstrate the feasibility of this approach, the circuit simulation based on parallel connected topology is carried out in ADS while the design and simulation of the fourth-order filter in dielectric technology in HFSS. Considerable sensitivity analysis is conducted to prove a better fabrication tolerance of the filter. In terms of implementation, this design technique will serve as a very useful mathematical tool for any filter design engineer.*

Keywords

Coupling matrix, chained function, dielectric resonator, parallel-connected, sensitivity, topology

1. Introduction

The parallel-connected network is generally used to achieve a higher-order filter due to its advantages in ease of tuning from the separated subnetworks of the filter [1]. This filter often possesses high sensitivity to fabrication tolerance because its design is usually based on Chebyshev polynomial approximation [2], [3]. The chained function, which transverse between Chebyshev and Butterworth polynomials, might be the trade-off and inherit the desired characteristics from both filters, which are studied in this paper to show their benefits in addressing the problem turning and filling in the gap [4], [5]. The Chebyshev filters have high rejection properties and an equal-ripple passband response to a specific filter order, making them the most common filter class in filter design [6], [7]. Once the appropriate characteristics polynomial satisfies the target filter specifications, the Chebyshev filter response requires a minimum tolerance to component value variations and a specific unloaded-Q factor for each resonator [1]. It should be noted that slight changes in the filter design parameter will cause the filter's target response to deviate, particularly at higher frequency bands [8]. Thus, pre-, and post-manufacturing tuning processes can be challenging, time-consuming, and expensive. Designing Chebyshev filters has always been challenging [9]. The chained function on the other hand can be found to compromise between Butterworth and Chebyshev approximations [10], [11] because it could combine the advantages of both Butterworth functions (lower filter losses, lower sensitivity, and lower resonator unloaded-Q factor) and Chebyshev functions (i.e., higher out-of-band and higher selectivity rejection) [12]. The technique of chained transfer functions can reduce filter complexity, manufacturing tolerance, and, most importantly, post-manufacturing tuning processes [4], [13]. This technique has the potential to extend the state-of-the-art development in a high-performance tuning-less filter toward higher operating frequencies and narrow bandwidth applications [5].

Parallel-connected two-port filter networks according to the Chebyshev function have been investigated, with various design concepts provided [14]. The two branch parallel-line networks were investigated and synthesized in [15], [16]. The mode admittance of two-port parallel networks has been reviewed using modal analysis in [17]. The eigenmode expansion approach was used to design parallel-connected networks for odd and even orders of Z and H matrices, respectively. The four-pole parallel-connected filter is designed and implemented in microstrip technology in [6], [21]. These design networks have been proven to have the advantages of simple coupling processes. Two-branch parallel networks will have the same number of couplings, regardless of how many transmission zeros are used in the filtering function F_N.

This paper presents a general design and synthesis technique of parallel-connected chained function filters. A general mathematical model according to the chained filtering function is derived and presented. Considerable comparison with the standard Chebyshev counterparts is included. Finally, the design and simulation of fourth-order chained function bandpass filter-based parallel connected

DOI: 10.13164/re.2023.0051

topology in dielectric technology and sixth-order filter using circuit simulation are presented.

The organization of this paper is as follows. Section 2 presents mathematical theory, synthesis technique, and circuit simulation results based on fourth and six-order chained filters. In Sec. 3 and 4, the design and simulation of parallel connected filter-based fourth-order dielectric resonators are presented. Section 5 presents the sensitivity analysis to prove a better fabrication tolerance of the filter is included, and finally, Section 6 presents the conclusion.

2. Synthesis Procedure

The parallel-branch network of an order N filter is proven to be the same regardless of how many transmission zeros are used in the filter's transfer function [1]. The synthesis procedure is fully discussed in this section. First, the low-pass network is synthesized into branches of sub-networks connected in parallel between the source and load using the event/odd-mode admittance expressions. Combining these will have a ladder network's characteristics. The design technique of this filter can be advantageous to many implementation methods, including dual-mode resonators.

Figure 1 shows the low-pass inverter coupled network according to chained. This network is synthesized, first, by computing the filtering function F_N, and solving S_{11}, and S_{21} in (1)–(3):

$$\left|S_{11}(\omega)\right|^2 = \frac{\varepsilon^2 F_N^2(\omega)}{1+\varepsilon^2 F_N^2(\omega)}, \tag{1}$$

$$\left|S_{21}(\omega)\right|^2 = \frac{1}{1+\varepsilon^2 F_N^2(\omega)} \tag{2}$$

where ω is a frequency variable, F_N is the filtering function, and ε is the ripple constant.

$$F_N = \frac{\alpha_4\omega^4 + \alpha_2\omega^2 + \alpha_0}{\beta_2\omega^2 + \beta_0}. \tag{3}$$

The resonators are set up in parallel configurations by splitting, using partial fraction expansion in [2].

2.1 Fourth-Order Chained Function Filter Synthesis

The filtering function is formed by chaining {2,2} order seed polynomial of Chebyshev polynomial of the first kind in (4).

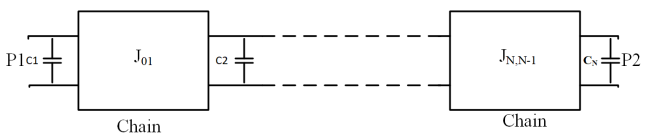

Fig. 1. The inverter-coupled low-pass chained network.

$$F_N = 4\omega^4 - 4\omega^2 + 1. \tag{4}$$

The zeros are obtained using the synthesis methods in [20] as

$$N(p) = p^8 - \mathrm{j}0.7637672096\,p + 1.172603940, \tag{5}$$

$$D(p) = 1.388721797\,p - \mathrm{j}1.060660172. \tag{6}$$

The even mode network is terminated by a unity admittance inverter hence, Y_e is computed using the technique in [20]

$$Y_e'(p) = \frac{1.388721797\,p - \mathrm{j}1.06066017}{p^2 + \mathrm{j}0.7637672096\,p + 1.172603940}. \tag{7}$$

Finally, partial fraction expansion in [20] is used to divide Y_e' into two parts; and the denominator is factorized as below.

$$Y_e'(p) = \frac{1}{1.080737547\,p + \mathrm{j}0.8282225677} + \frac{1}{2.1578335886\,p - \mathrm{j}3.301737005}. \tag{8}$$

The same method can be applied to the odd-mode admittance network, with the same results as

$$Y_o'(p) = \frac{1}{1.080737547\,p - \mathrm{j}0.8282225677} + \frac{1}{2.1578335886\,p + \mathrm{j}3.301737005}. \tag{9}$$

The new parallel network shown in Fig. 2 is formed using the new admittance expressions for even modes. The corresponding circuit simulation response is shown in Fig. 4 and the component's values derived are summarized in Tab. 1. The J-admittance values are the numerator values, and the capacitance is the denominator values of (8) and (9). This design technique can be useful in synthesizing circuits in different parallel configurations, such as four and six-branch parallel networks, by further breaking down the even-mode admittance, Y_e. The low-pass network can then be transformed into a bandpass network using the appropriate transformation equations in [7], [9], [22]. The band-pass network is shown in Fig. 3 and the corresponding S-parameter response in Fig. 5. The ability of this technique to select several parallel branches is beneficial when designing filters because it allows designers to place the resonators in the circuit. This technique applies to odd symmetrical higher-order filter networks.

Components	{1,1,2}	{1,3}	{2,2}
$C_1 = C_2$	0.8213 F	2.1142 F	1.0807 F
$C_3 = C_4$	1.605 F	1.0322 F	2.1578 F
$J_{S1} = J_{2L}$	1	1	1
$J_{S3} = J_{4L}$	1	1	1
J_{12}	–0.7380	3.1954	0.8282
J_{34}	2.8164	–0.7616	–3.3023

Tab. 1. The chained function component values of the fourth-order network.

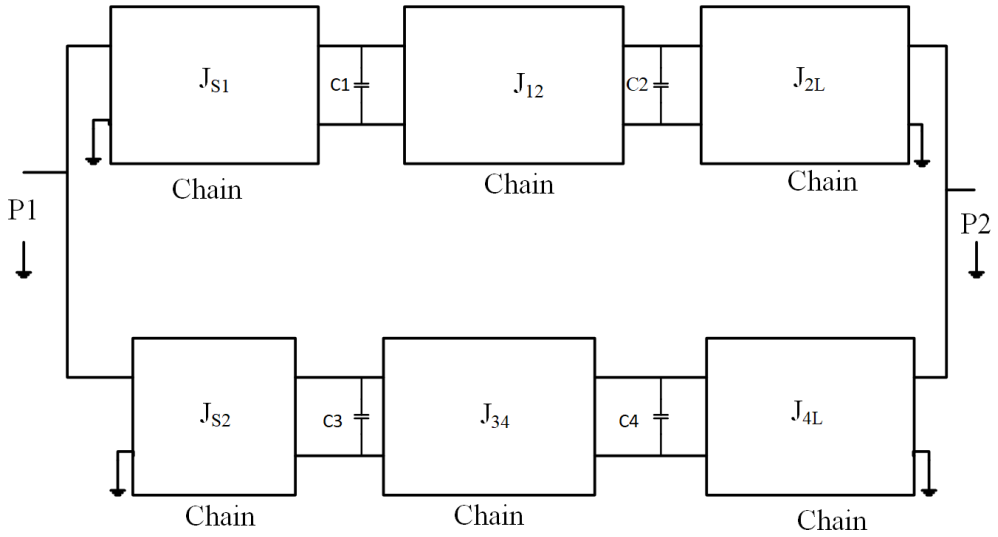

Fig. 2. The fourth-order chained parallel branch low-pass network.

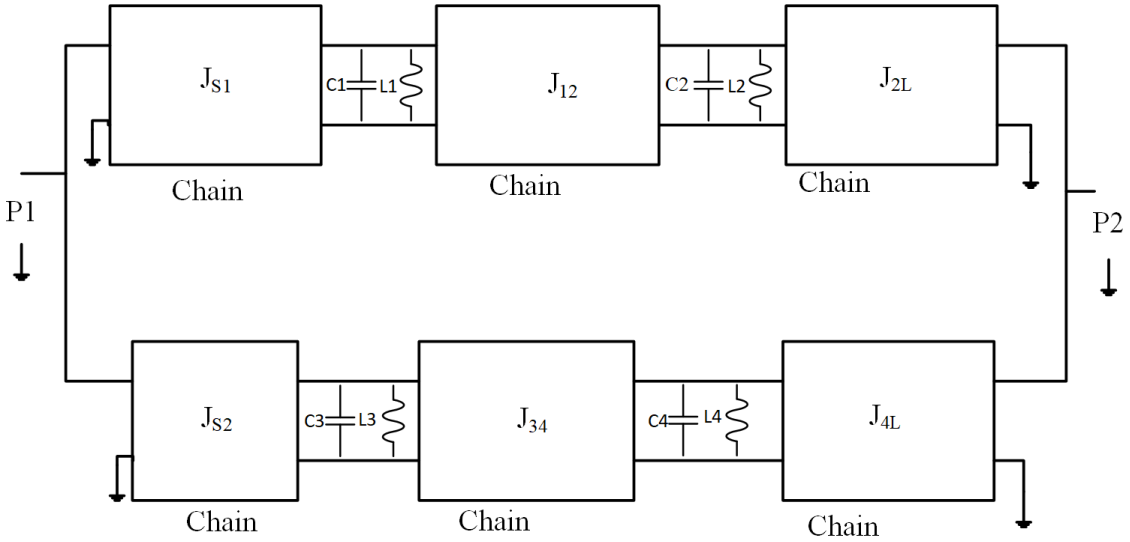

Fig. 3. Fourth order chained parallel branch bandpass network.

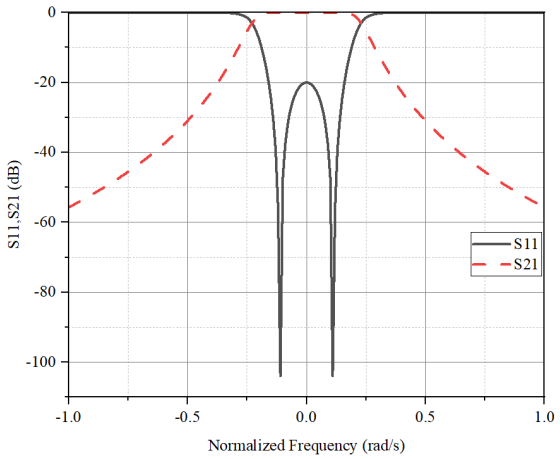

Fig. 4. The simulation response of fourth order low-pass network.

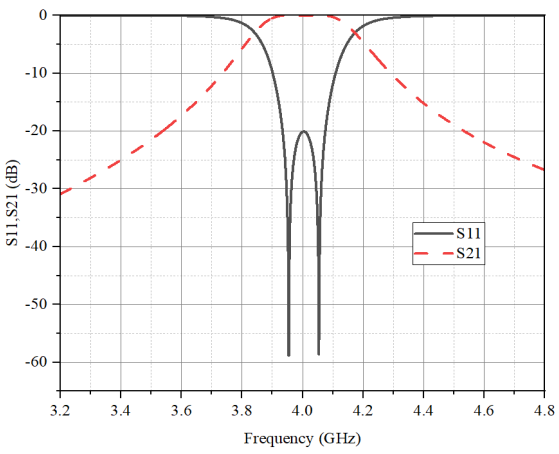

Fig. 5. The simulation response of fourth-order bandpass network.

2.2 Sixth-Order Chained Function Filter Synthesis

The filtering function of the sixth-order filter can be formed by chaining {2,2,2} seed-order of Chebyshev polynomial of the first kind in (10):

$$F_N(\omega) = 8\omega^6 - 12\omega^4 + 6\omega^2 - 1. \quad (10)$$

The zeros are obtained using the synthesis methods in [20] as

$$N(p) = 1.555186313p^2 + \mathrm{j}1.022759991p + 0.7500000, \quad (11)$$

$$D(p) = p^3 - \mathrm{j}0.6576446734p^2 + 1.743053976p - \mathrm{j}0.8291561977. \quad (12)$$

The even mode network is terminated by a unity admittance inverter hence, Y_e is computed using the technique in [20]

$$Y_e'(p) = \frac{p^3 - \mathrm{j}0.6576446734p^2 + 1.743053976p - \mathrm{j}0.8291561977}{1.555186313p^3 - \mathrm{j}1.022759995 + 0.75000000}. \quad (13)$$

Finally, partial fraction expansion in [1] is used to divide into two parts. And the denominator is factorized as in (14)

$$Y_e'(p) = \frac{1}{1.982p - \mathrm{j}0.8708} + \frac{1}{1.5534p + \mathrm{j}1.9510} + \frac{1}{2.5456p + \mathrm{j}3.7217}. \quad (14)$$

The new parallel network shown in Fig. 6 is formed for the sixth-order filter using the admittance expressions for even modes in (14). The circuit simulation S-parameter response is shown in Fig. 7 side by side with the Chebyshev response shown in Fig. 8.

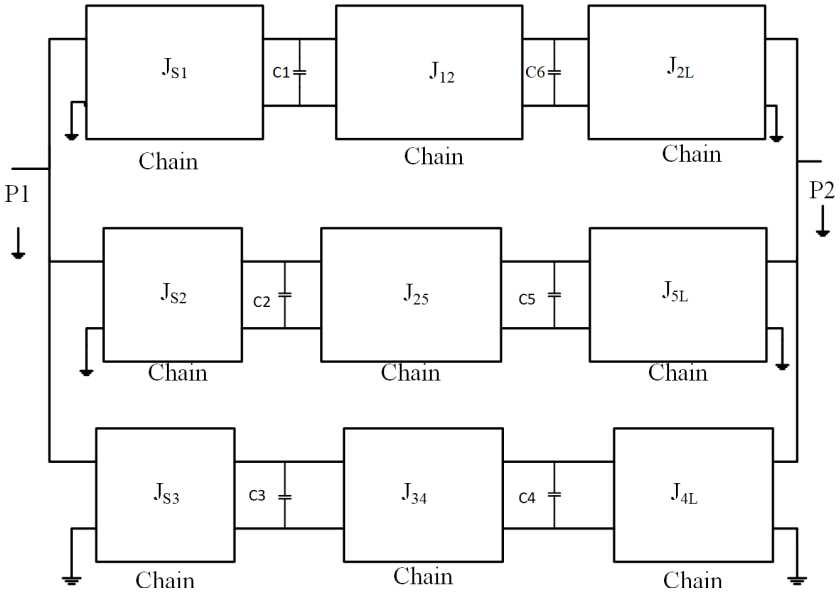

Fig. 6. The sixth order chained parallel branch low-pass network.

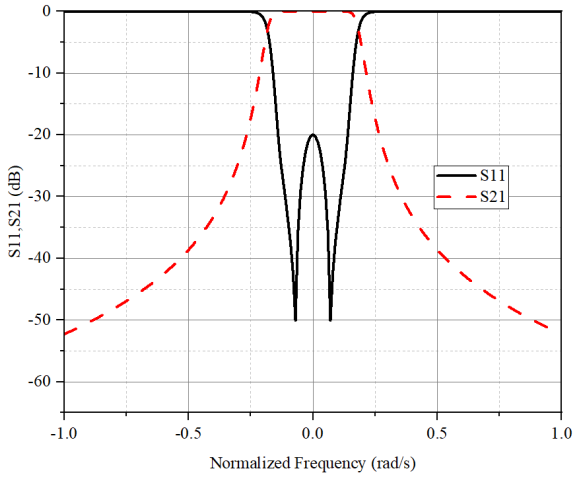

Fig. 7. The simulation response of sixth order chained network.

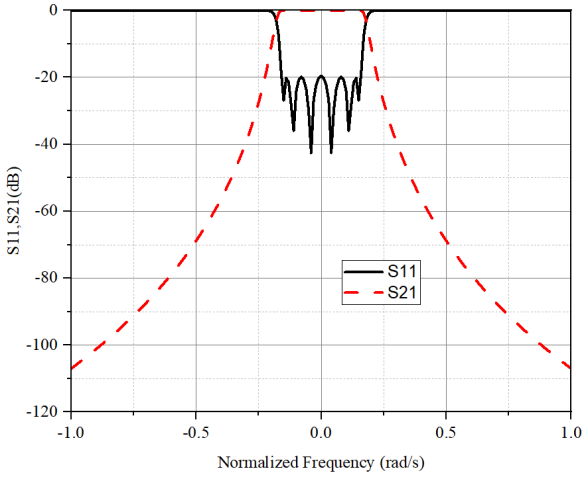

Fig. 8. The simulation response of sixth order Chebyshev network.

Components	{2,2,2}	{2,2}
$C_1 = C_6$	1.982 F	2.0984 F
$C_2 = C_5$	1.553 F	1.9798 F
$C_3 = C_4$	2.546 F	3.5225 F
$J_{S1} = J_{S2} = J_{S3}$	1	1
$J_{S4} = J_{S5} = J_{S6}$	1	1
J_{16}	–0.8708	–0.8047
J_{25}	1.9509	2.1834
J_{34}	–3.7217	–4.6442

Tab. 2. The chained function component values of sixth order network.

The component values are summarized in Tab. 2. This approach can be used to directly synthesize a parallel-connected symmetrical two-port network. It has no limitations when compared to the technique described in the literature [5], [24].

2.3 Coupling Matrix Analysis

The filter coupling matrix can be computed using (15) and (16):

$$y_{11}(s) = \sum_{k=1}^{N} \frac{T_{Nk} T_{1k}}{\omega - \lambda_k}, \tag{15}$$

$$y_{22}(s) = \sum_{k=1}^{N} \frac{T_{Nk^2}}{\omega - \lambda_k}. \tag{16}$$

The traditional ladder network is replaced by the coupling matrix synthesis and similarity transformation technique in [14], [18]. A series of similarity transformations are carried out to enable the complex coupling matrix to be rearranged until a more suitable coupling configuration that is physically realizable is attained. The full $N+2$ coupling matrix achieved after transformation is presented in (21), this represents the filter's lowpass prototype described in [19], [23].

To achieve the desired coupling matrix topology, a reduction procedure can be used on the coupling matrix [3]. The first and last rows of the matrix can be determined. The orthogonal rows can be constructed using the Gram-Schmidt orthogonalization process [3]. The coupling matrix of sub-networks $\mathbf{M}_{14}$ and $\mathbf{M}_{23}$ are formed using the techniques described in [4]. Similarity transformation is used on the sub-network matrix in (17) and (18) to obtain the coupling combination in (19) and (20). Finally, the full coupling matrix, $\mathbf{M}$, which includes the coupling from the source and the load, can be formulated [4]. The realizable prototype routing structure is shown in Fig. 9.

$$\mathbf{M}_{14} = \begin{pmatrix} 0 & 0.48134 & -0.48137 & 0 \\ 0.48134 & 1.53012 & 0 & 0.48137 \\ -0.48137 & 0 & -1.53012 & 0.48137 \\ 0 & 0.48137 & 0.48137 & 0 \end{pmatrix}, \tag{17}$$

$$\mathbf{M}_{23} = \begin{pmatrix} 0 & -0.68018 & 0.68018 & 0 \\ -0.68018 & 0.76635 & 0 & 0.68018 \\ 0.68018 & 0 & -0.76635 & 0.68018 \\ 0 & 0.68018 & 0.68018 & 0 \end{pmatrix}, \tag{18}$$

$$\mathbf{M}_{14} = \begin{pmatrix} 0 & 0.68076 & 0 & 0 \\ 0.68076 & 0 & 1.53012 & 0 \\ 0 & 1.53012 & 0 & 0.68076 \\ 0 & 0 & 0.68076 & 0 \end{pmatrix}, \tag{19}$$

$$\mathbf{M}_{23} = \begin{pmatrix} 0 & 0.96192 & 0 & 0 \\ 0.96192 & 0 & 0.76635 & 0 \\ 0 & 0.76635 & 0 & -0.96192 \\ 0 & 0 & -0.96192 & 0 \end{pmatrix}, \tag{20}$$

$$\mathbf{M} = \begin{pmatrix} 0 & 0.68076 & 0.96192 & 0 & 0 & 0 \\ 0.68076 & 0 & 0 & 0 & 1.53012 & 0 \\ 0.96192 & 0 & 0 & 0.76635 & 0 & 0 \\ 0 & 0 & 0.76635 & 0 & 0 & -0.96192 \\ 0 & 1.53012 & 0 & 0 & 0 & 0.68076 \\ 0 & 0 & 0 & -0.96192 & 0.68076 & 0 \end{pmatrix}. \tag{21}$$

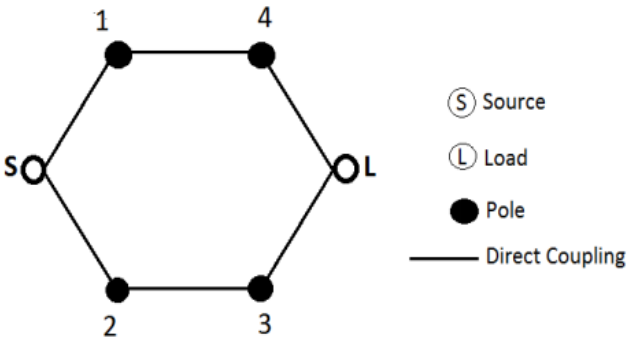

Fig. 9. The coupling routing structure of the filter.

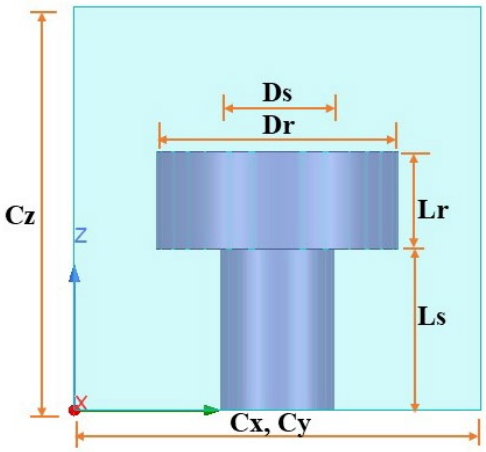

Fig. 10. Dielectric resonator inside an enclosure configuration.

Parameter	Dimension
Resonator Puck	$\varepsilon_r = 34$, $D = 14.4$ mm, $L_r = 5.89$ mm
Resonator Support	$\varepsilon_{rs} = 10$, $D_s = 6.87$ mm, $L_s = 9.88$ mm
Resonator Enclosure	$C_x = C_y = 24.88$, $C_z = 24.55$

Tab. 3. Dielectric resonator dimensions.

3. Dielectric Resonator Configuration

Figure 10 shows a dielectric resonator mounted inside a squared cavity which is assumed to have a parameter label as cavity width (C_x, C_y), cavity length C_z, resonator diameter (D_r), resonator height (L_r), low permittivity dielectric support diameter (D_s), and support height (L_s). The chosen dielectric resonator is cylindrical and has a low dielectric permittivity. The design parameters are shown in Tab. 3.

3.1 Dielectric Resonator Electric-Field Distribution

The model is analyzed under eigenmode in high-frequency simulation software (HFSS) to find out the TE mode and TM mode for waves to propagate. TE and TM mode refers to the transverse mode of electromagnetic radiation [18]. The transverse mode will only happen when there is neither an electric field nor a magnetic field in the direction of wave propagation. In each of the designs, the first four eigenmodes were recorded, and they represent the single modes (TEH and TME mode) and the dual hybrid modes (HEH and HEE mode). The third index of these modes is used to distinguish in both modes even and odd symmetry along the resonator's axis at $Z = L/2$. An "E" represents electrical wall symmetry, while an "H" represents magnetic wall symmetry [20]. The E-distribution diagrams for these modes are shown in Figs. 11 and 12 (left and right), plotted for the first two single modes (TEH and TME modes) of the cylindrical puck on the low permittivity dielectric support inside the cavity enclosure.

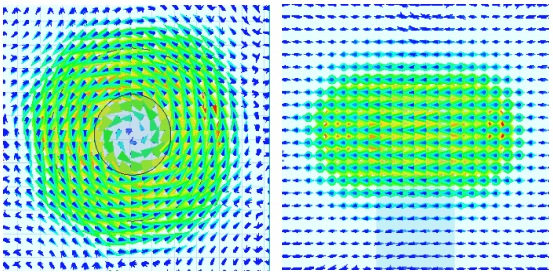

Fig. 11. The electric-field distribution of the single-mode TEH - 4.00023 GHz.

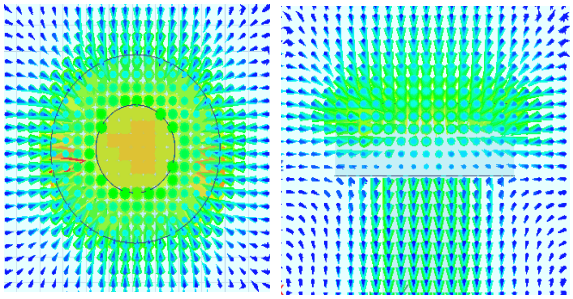

Fig. 12. The electric-field distribution of the single-mode TME - 4.72553 GHz.

3.2 Mode-Chart of Dielectric Resonator

The eigenmode solver window in HFSS is used to generate the mode chart as proof of the design idea. By increasing the resonator puck diameter to height ratio, the simulation was run multiple times. The diameter remained constant while the size of the resonator puck was reduced by half. It can be observed that as the ratio of D/L increases, the resonant frequencies of each mode will increase accordingly. This shows that the resonant frequency can be designed to the desired frequency by adjusting the ratio of D/L. Figure 13 shows the resulting mode chart diagram for the first four modes of the dielectric resonator while Table 4 summarizes the coupling coefficient values.

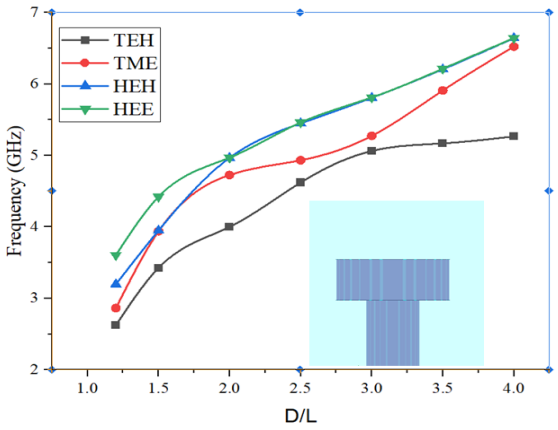

Fig. 13. The mode chart of the first four dielectric resonator modes.

W (mm)	f_1 (GHz)	f_2 (GHz)	K
1	4.00014	4.00826	0.002027869
1.8	3.99936	4.01147	0.003023400
2.6	3.98933	4.00385	0.003633085
3.4	3.98617	4.00348	0.004333086
4.2	3.98440	4.00449	0.005029453
5.8	3.97872	4.00384	0.006293658
6.5	3.97491	4.00276	0.006981903
7.4	3.97953	4.01050	0.007752045
8.2	3.96911	4.00263	0.008409559
8.8	3.96546	4.00187	0.009139634
9	3.96542	4.00186	0.009147222

Tab. 4. Summary of coupling coefficient (K) and iris width (W) values.

3.3 Dielectric Resonator Coupling

Achieving good coupling between resonators is based on extracting the external quality factor (Q_e) and coupling coefficient (K) to form a parallel-connected network using (22) and (23). We begin by investigating the coupling

between two resonators that are symmetrically divided into separate resonators and terminated by either an electric wall or a magnetic wall. The coupling is determined by using the resonance frequency of the two distinct resonators. The coupling matrix **M** elements are normalized to the fractional bandwidth. Matrix **M** is a coupling element between two adjacent resonators. The values obtained for f_1 and f_2, as well as the corresponding coupling factor K, are summarized in Tab. 4. Figure 14 shows the two coupled resonators together with their corresponding plot of coupling coefficient K versus W. Figure 15 shows two coupled resonator structures and their corresponding plot of Q_e versus the length of probe L obtained in HFSS. The original cavity dimensions are used to find the resonant frequencies for both even and odd modes in HFSS.

$$Q_e = \frac{f_0}{BW \times R_1}, \tag{22}$$

$$K = \frac{f_0}{BW} \times \frac{f_2^2 - f_1^2}{f_2^2 + f_1^2}. \tag{23}$$

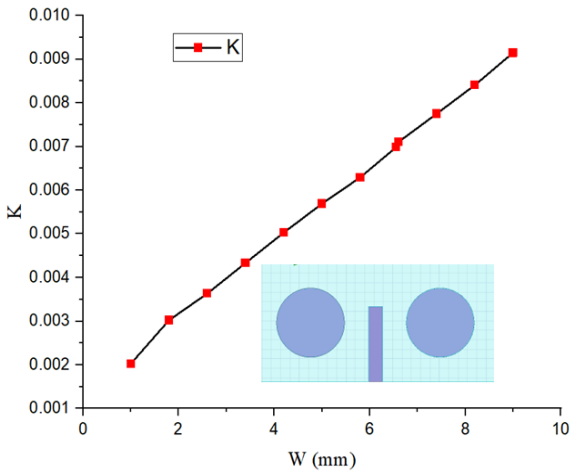

Fig. 14. The coupling K plot against the width iris W.

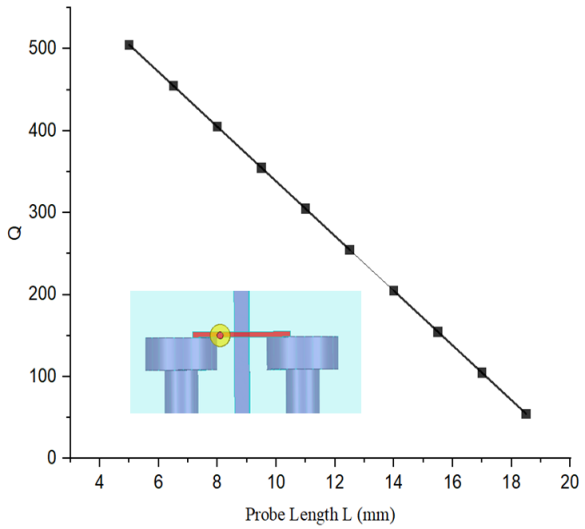

Fig. 15. Quality factor Q plot against the length probe L.

The first eigenmode frequency is f_1, the second eigenmode frequency is f_2, and f_0 is the center frequency.

In Fig. 14, it can be noticed that the coupling gap W increases, as the coupling coefficient K increases and vice-versa. The weaker coupling results in a lower coupling coefficient and a strong coupling in a higher coupling coefficient.

4. Filter Design and Simulation

The filter design and simulation are carried out using ANSYS HFSS driven-model approach. The chained-function polynomial $F_N(\omega) = 4\omega^4 - 4\omega^2 + 1$ with the seed function of order {2,2} is transformed into a parallel network using dielectric resonators. The cut-off frequency of the filter is 3.0559 GHz, the center frequency is 4 GHz, the filter return loss is 20 dB, and a fractional bandwidth of 0.5%. Figures 16 and 17 show the 3D designed structural setup of the bandpass filter with and without E-field distribution. The iris thickness is maintained at 3 mm for all irises. The design is carried out by adjusting the dimension of one resonator branch with the connecting irises, and the

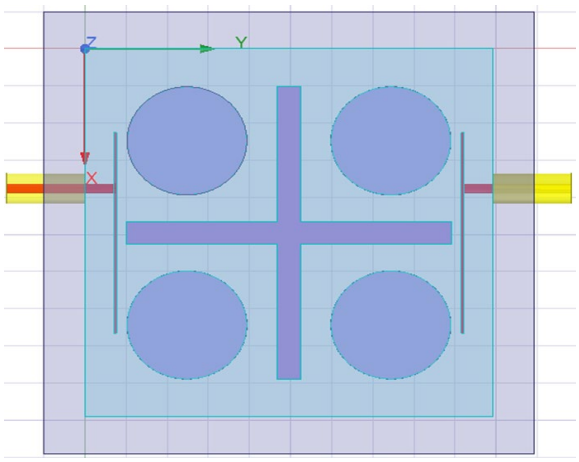

Fig. 16. Parallel-connected chained dielectric resonator filter 3D topology.

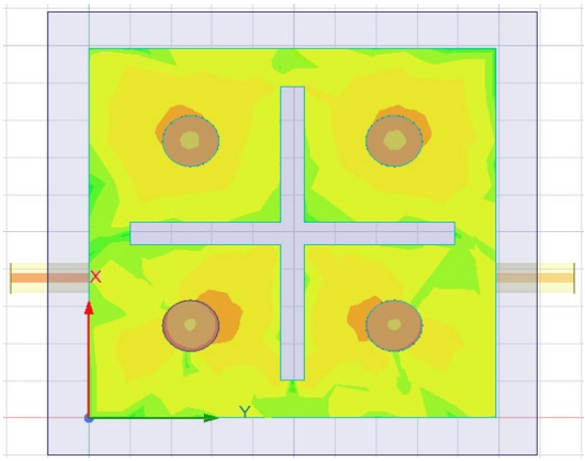

Fig. 17. Parallel-connected chained dielectric resonator filter 3D topology with E-field distribution.

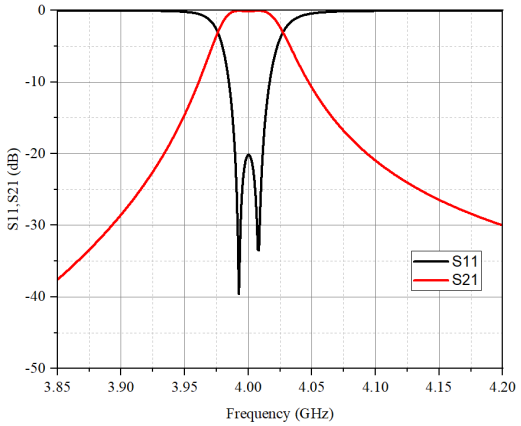

Fig. 18. The simulation response of the dielectric resonators network.

input probe until the desired response is attained. The process is repeated by inserting the output probe and the next resonator's branch at the same time. The final parameters of the topology after tuning process are $D_1 = D_2 = D_3 = D_4 =$ 14.602 mm, $W_{12} = W_{34} = 5.01$ mm and $W_{14} = W_{23} =$ 5.1 mm.

The achievable S-parameter response of the filter is shown in Fig. 18. The center frequency is 4 GHz, fractional bandwidth of 0.5%, and a return loss level of 20 dB. The rejection is better than 20 dB below 3.94 GHz and above 4.055 GHz. The results are in good agreement with the theory.

4.1 The Filter Loss Consideration

To develop a filter, the required attenuation specifications must be considered, with special attention given to insertion loss dissipation at the center of the passband. For multiple resonator minima unloaded Q is required to realize the design. Effects of losses on the filter's insertion loss response are of particular interest, particularly when working with finite resonator values. The insertion loss at the filter passband due to dissipation for multiple resonators can be computed using (24).

Seed functions orders	Seed-function combination	Loss (25 dB)	Loss (20 dB)	Loss (15 dB)
4	{1,1,1,1}	5.2839	5.4461	5.7163
3	{1,1,2}	5.5000	5.6730	5.9324
2	{2,2}	5.8163	6.2567	6.3882
2	{3,1}	6.1363	6.3961	6.5360
1	{4}	6.2567	6.7970	6.9514

Tab. 5. The dielectric resonator filter losses at various RL values.

$$L_0 = \frac{3.343 f_0}{Q_{\mathrm{uL}} \Delta f} \sum_{i=1}^{n} g_i \tag{24}$$

where Δf is the bandwidth, f_0 the center frequency, g_i (i = 1, 2..., N) represents the i-th low-pass prototype element value, and Q_{uL} is the unloaded-Q factor of each resonator.

Table 5 shows the calculated values for the chained-function filter loss for various seed-order combinations. The table's first row represents the Butterworth approximation normalized to the same ripple bandwidth, and the last row corresponds to the traditional Chebyshev approximation. It can be observed that for identical resonators and fixed fractional bandwidth, the filter loss increases with an increase in filter elements. The chained function filter loss is slightly less than that of conventional Chebyshev and higher than the Butterworth filter; this could be robust in terms of sensitivity to manufacturing tolerance and usage in any given environment. The filter RL level can be used to determine the loss values for both chained-function and conventional Chebyshev filters.

5. The Filter Sensitivity Analysis

Fabrication tolerance analysis is carried out on the parallel connected chained function dielectric resonator bandpass using ANSYS HFSS. This is to prove that the filter can be produced with better tolerance compared to the conventional Chebyshev filters. Several experiments were conducted, where the values of resonator diameter, length, iris thickness, and enclosure size are changed to have a difference of ±0.5%, ±1%, and ±2% to assess the effects of manufacturing tolerance shown in Tab. 6. The distribution's variance was chosen to provide a maximum error of approximately 5 µm. The results from different experiments conducted on the filters of order four are presented in Figs. 19 to 22. The return loss shift in the passband is recorded to be ±0.07% and ±0.025% compared to its original values. Similarly, the same experiment is conducted on a standard Chebyshev filter of the same order using ADS software by changing its component values. The shift in RL is recorded to be ±1.8% and ±2.1% compared to the original values in Figs. 23 to 26.

For all cases, the RL remains at 20 dB. These findings greatly prove that parallel-connected chained function filters are less sensitive to manufacturing tolerances while preserving selectivity. This is exhibited by the lower percentage change in return loss distributions for chained function filters. The further apart separation of the filter poles is evident confirming higher manufacturing tolerance. Table 7 compares the results of this work with previous works.

Parameters	Original Value (mm)	Value Change %						Return Loss
		+0.5%	+1%	+2%	–0.5%	–1%	–2%	Change (%)
Resonator Diameter (D)	14.606	14.6750	14.74802	14.89404	14.52899	14.45598	14.30996	±0.07
Resonator Length (L_d)	5.88	5.9094	5.9388	5.9976	5.8506	5.8212	5.7624	±0.025
Iris Thickness (T)	3	3.015	3.03	3.06	2.985	2.97	2.97	±0.07
Enclosure Size $C_x = C_y = C_z$	24.8	24.924	25.048	25.296	24.6776	24.552	24.305	±0.025

Tab. 6. Percentage changes for resonator diameter, resonator length, iris thickness, and enclosure values of 4th-order parallel-connected chained function filter.

Refs	Implementation technology	Filtering function	f_0 (GHz)	BW (MHz)	IL (dB)	RL (dB)
[2]	Microstrip	Chained	2.4	150	1	15
[22]	Microstrip	Chebyshev	4.63	400	1.808	9.995
[23]	Microstrip	Chebyshev	16	500	0.1	15.573
[24]	Microstrip	Chebyshev	3.5	300	0.9	22
This work	Dielectric	Chained	4	200	0.98	20

Tab. 7. Simulation results compared with previous work.

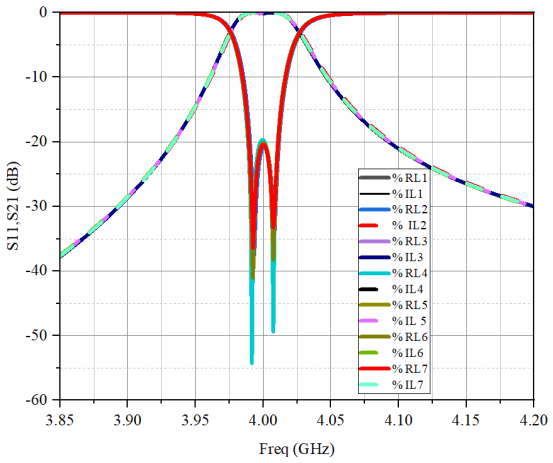

Fig. 19. The effect of tolerance on the dielectric resonator diameter.

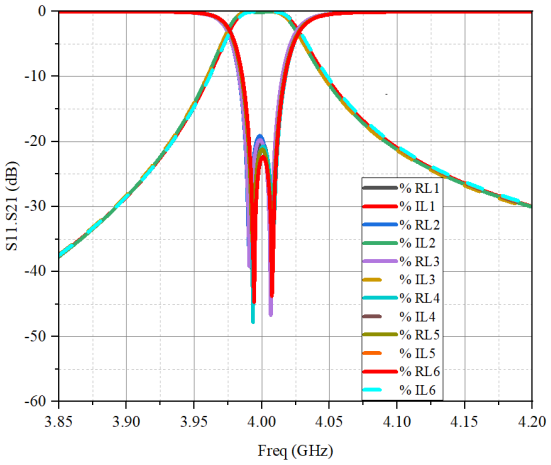

Fig. 21. The effect of tolerance on the dielectric iris thickness.

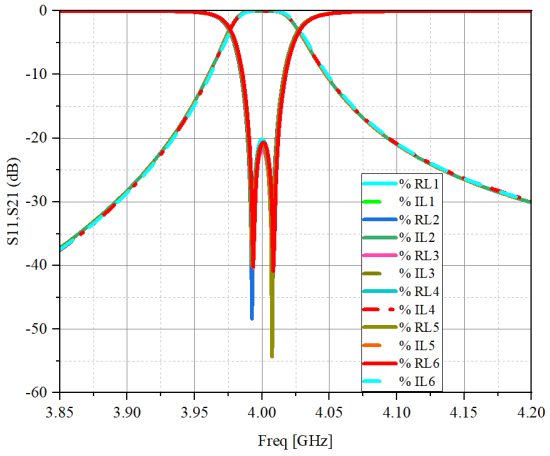

Fig. 20. The effect of tolerance on the dielectric resonator length.

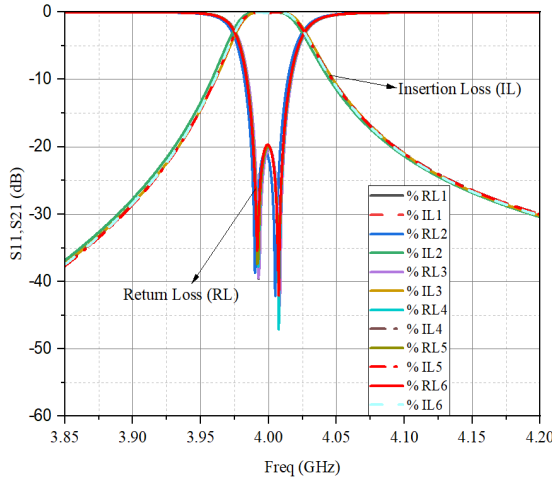

Fig. 22. The effect of tolerance on the enclosure size.

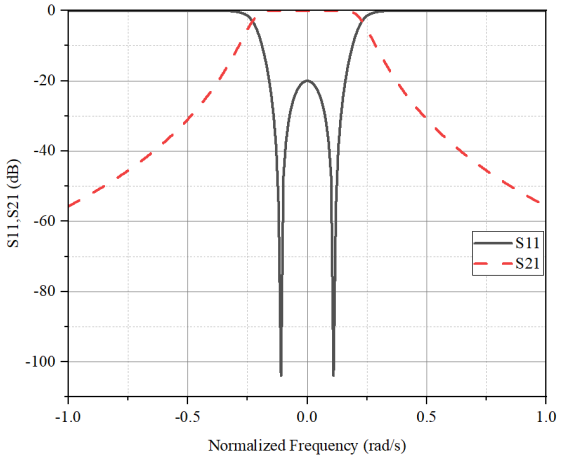

Fig. 23. The fourth order chained original filter response.

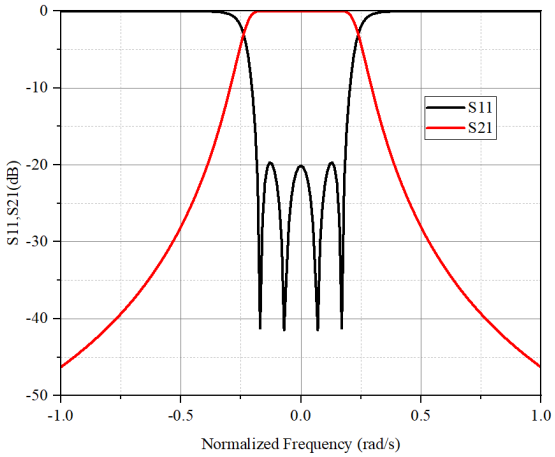

Fig. 24. The fourth order Chebyshev original filter response.

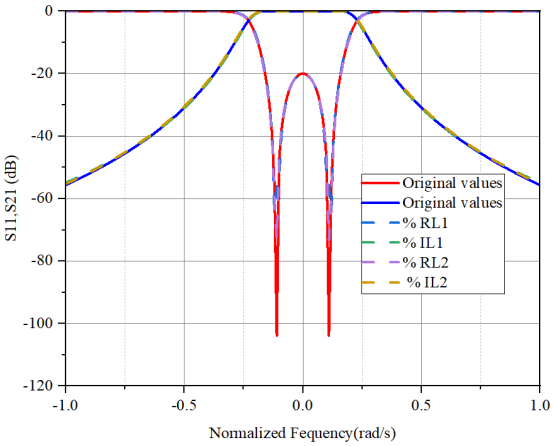

Fig. 25. The effect of tolerance on fourth-order chained filter component values.

5.1 Fourth Order {2,2} Chained versus Third and Fourth-Order Chebyshev Filter

Compared to the third and fourth order Chebyshev filter's numerical response in Fig. 27, the chained function filter out-of-band rejection is higher than the third order Chebyshev but less than the fourth order. The chained function passband has only poles as expected for an implementation. The poles of the parallel-connected chained filter are placed farther apart than those of the third-order Chebyshev response. This is the main benefit of chained-function polynomial it efficiently sets multiple RL zeros at the same frequencies, resulting in the filter being less sensitive to manufacturing tolerance while maintaining the required out-of-band rejection.

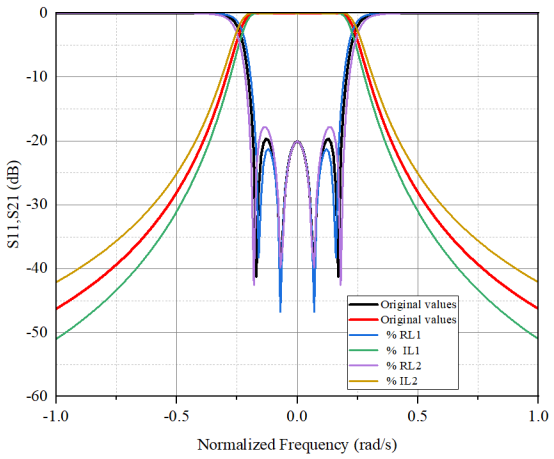

Fig. 26. The effect of tolerance on the fourth order Chebyshev filter component values.

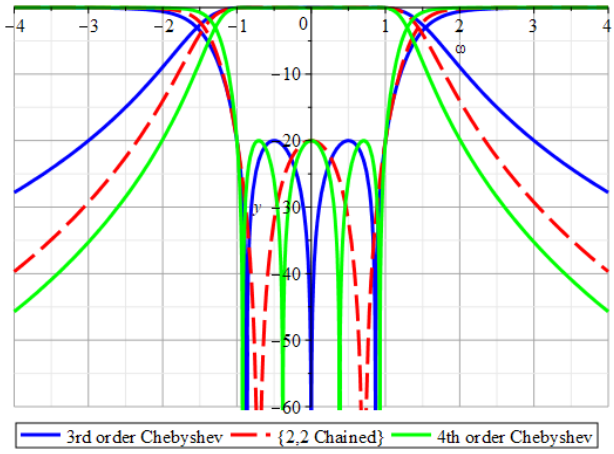

Fig. 27. Comparison plots of {2,2} order chained versus 3rd-order and 4th-order Chebyshev filter response.

6. Conclusion

We presented a design and synthesis technique for a parallel-connected dielectric filter using a chained-function polynomial in this paper. The technique is based on the even-mode admittance of the chained function to form the parallel network, in which the low-pass network is synthesized into sub-networks branches connected in parallel using the even-mode admittance expression obtained. A general transfer function FN according to chained was derived for fourth and sixth-order filters. This technique gives more flexibility in arranging the resonators and choosing the number of the required parallel branches for

synthesis. The feasibility of this approach was demonstrated using circuit simulation in ADS, while a fourth order dielectric resonator was designed and simulated using ANSYS HFSS. Sensitivity analysis is carried out using HFSS to prove a better fabrication tolerance of the filter. The results indicate low sensitivity as the position of the reflection zero is slightly affected by tolerance. The results realized from the theory agree well with simulation models. In terms of implementation, it will serve as a very useful mathematical tool for any filter design engineer.

Acknowledgments

The authors would like to thank YUTP (015LC0-320) for providing the funding that allows this research to be viable and successful. The authors also appreciate all individuals who have contributed directly or indirectly to complete this project.

References

[1] HUNTER, I. C., BILLONET, L., JARRY, B., et al. Microwave filters - Applications and technology. *IEEE Transactions on Microwave Theory and Technique*, 2002, vol. 50, no. 3, p. 794 to 805. DOI: 10.1109/22.989963

[2] CHUAN, C. Y., CHEAB, S. Design and synthesis of parallel connected chained function filter. In *APACE 2019 - 2019 IEEE Asia-Pacific Conference on Applied Electromagnetics.* Malacca (Malaysia), November 2019, p. 1–4. DO1: 10.1109/APACE47377.2019.9020899

[3] CHEAB, S., WONG, P. W., SOEUNG, S. Design of multi-band filters using parallel connected topology. *Radioengineering*, 2018, vol. 27, no. 1, p. 186–192. DOI: 10.13164/re.2018.0186

[4] LIM., Y. P., CHEAB, S., SOEUNG, S., et al. On the design and fabrication of chained-function waveguide filters with reduced fabrication sensitivity using CNC and DMLS. *Progress in Electromagnetics Research B*, 2020, vol. 87, p. 39–60. DOI: 10.2528/PIERB20011101

[5] CHRISOSTOMIDIS, C. E., LUCYSZYN, S., On the theory of chained-function filters. *IEEE Transactions on Microwave Theory and Technique*, 2005, vol. 53, no. 10, p. 3142–3151. DOI: 10.1109/TMTT.2005.855358

[6] CAMERON, R. J., YU, M., WANG, Y. Direct-coupled microwave filters with single and dual stopbands. *IEEE Transactions on Microwave Theory and Technique*, 2005,vol. 53, no. 11, p. 3288 to 3297. DOI: 10.1109/TMTT.2005.859032

[7] ZHANG, Y., WU, K. L. General method for synthesizing dispersive coupling matrix of microwave bandpass filters. *International Journal of Microwave Wireless Technologies*, 2022, vol. 14, no. 3, p. 379–386. DOI: 10.1017/S1759078721000672

[8] QI, L., XING, D., WANG, R., et al. Coupling matrix synthesis of general Chebyshev filters. In *MATEC Web of Conferences*, 2020, vol. 309, p. 1–6. DOI: 10.1051/matecconf/202030901011

[9] CAMERON, R. J. Synthesis of a general class of the Chebyshev filter function (6.1 Polynomial forms of the transfer and reflection parameters S_{21} and S_{11} for a two-port network). Chapter 6 in CAMERON, R. J., KUDSIA, C. M., MANSOUR, R. R. *Microwave Filters for Communication Systems*. 2nd ed. Wiley, 2018, p. 177–213. DOI: 10.1002/9781119292371.ch6

[10] ZHU, L., PAYAPULLI, R., SHIN, S. H., et al. 3-D printing quantization predistortion applied to sub-THz chained-function filters. *IEEE Access*, 2022, vol. 10, p. 38944–38963. DOI: 10.1109/access.2022.3162586

[11] BONG, D. C. H., JEOTI, V., CHEAB, S., et al. Design and synthesis of chained-response multiband filters. *IEEE Access*, 2019, vol. 7, p. 130922–130936. DOI: 10.1109/access.2019.2940059

[12] LIM, Y. P., TOH, L., CHEAB, S., et al. Chained-function waveguide filter for 5G and beyond. In *IEEE Region 10 Annual International Conference TENCON 2019*. Jeju (South Korea), 2019, p. 107–110. DOI: 10.1109/TENCON.2018.8650548

[13] PERENIC, G., STAMENKOVIC, N., STOJANOVIC, N., et al. Chained-function filter synthesis based on the modified Jacobi polynomials. *Radioengineering*, 2018, vol. 27, no. 4, p. 1112 to 1118. DOI: 10.13164/re.2018.1112

[14] CAMERON, R. J., KUDSIA, C. M., MANSOUR, R. R. Tunable filters. Chapter 22 in CAMERON, R. J., KUDSIA, C. M., MANSOUR, R. R. *Microwave Filters for Communication Systems*. 2nd ed. Wiley, 2018, p. 731–783. DOI: 10.1002/9781119292371.ch22

[15] AB WAHAB, N., HIDAYAT, N. M., ISMAIL KHAN, Z., et al. Two parallel-coupled rings for narrow bandpass filter application. *Journal of Telecommunication Electronics and Computer Engineering*, 2016, vol. 8, no. 3, p. 73–77. ISSN: 2180-1843

[16] CHEAB, S., WONG, P. W., CHEW, X. Y. Parallel connected dual-mode filter. *IEEE Microwave and Wireless Components Letters*, 2015, vol. 25, no. 9, p. 582–584. DOI: 10.1109/LMWC.2015.2451393

[17] POMMIER, V., CROS, D., GUILLON, P., et al. Transversal filter using whispering gallery quarter cut resonators. In *2000 IEEE MTT-S International Microwave Symposium Digest*, 2000, vol. 3, p. 1779–1782. DOI: 10.1109/MWSYM.2000.862324

[18] CAMERON, R. J. Resonant frequency calculation in dielectric resonators. Chapter 16 in CAMERON, R. J., KUDSIA, C. M., MANSOUR, R. R. *Microwave Filters for Communication Systems*. 2nd ed. Wiley, 2018, p. 517–544. DOI: 10.1002/9781119292371.ch16

[19] SONI, S., GHADIYA, A., SHUKLA, N. A new approach for the coupling identification in dielectric resonators filters. In *Proceedings of the 2014 4th International Conference on Communication Systems and Network Technologies CSNT 2014*. Bhopal (India), 2014, p. 30–33. DOI: 10.1109/CSNT.2014.15

[20] DUBEY, C., MAHMOOD, R. Review on dielectric resonator filter. In *Proceedings of National Conference on Recent Advances in Electronics and Communication Engineering, RACE-2014*. Greater Noida (UP, India), 2014, p. 1–7.

[21] HUNTER, I. *Theory and Design of Microwave Filters (IEEE Electromagnetic Wave Series No.48).* United Kingdom, Unversity Press Cambridge, 2006, p. 81–84. ISBN: 0852967772

[22] SASIC, M., IMECI, S. T. Design of microstrip coupled-line bandpass filter. *Heritage and Sustainable Development*, 2021, vol. 3, no. 1, p. 44–52. DOI: 10.37868/hsd.v3i1.55

[23] SHARMA, S. S., SHARMA, S. Design and simulation of sixth order parallel coupled line band pass Chebyshev filter. *International Journal for Research in Applied Science & Engineering Technology (IJRASET)*, 2015, vol. 3, no. V, p. 906 to 910. ISSN: 2321-9653

[24] AL-YASIR, Y. I. A., OJAROUDI PARCHIN, N., ALABD-ALLAH, A., et al. Design, simulation and implementation of very compact open-loop trisection BPF for 5G communications. In *2019 IEEE 2nd 5G World Forum (5GWF).* Dresden (Germany), 2019, p. 189–193. DOI: 10.1109/5GWF.2019.8911677

About the Authors ...

Francis E. CHINDA (corresponding author) was born in 1983. He received his B.Eng. (Honors) degree in Electrical and Electronic from the prestigious University of Maiduguri, Nigeria. He completed his MSc. from the University of Nottingham, UK in 2015 and currently is pursuing a Ph.D. at Universiti Teknologi PETRONAS in Malaysia. His research interests include the design and synthesis of bandpass filters for 5G and satellite applications.

Sovuthy CHEAB (M'15) holds a B.Eng. (Hons) in Electrical and Electronic Engineering, M.Sc. and Ph.D. in RF and Microwave Engineering from Universiti Teknologi Petronas. Before going into industry, he worked as a lecturer for 6 years in Electrical and Electronic Engineering Department, UTP teaching electromagnetic theory, communication systems, and RF/microwave related subjects. He had supervised a total of 6 Ph.D. and 7 master students. In terms of research, he had secured many national and industry grant projects. Dr. Cheab has been an Executive Committee Member of the IEEE ED/MTT/SSC Penang Chapter, since 2016, and had been elected as the secretary of the Chapter for 2021 to 2022 term. He served as the secretary of IMESS 2018, MTT Technical Chair of IMESS 2019 and the Publication Chair of ICIAS 2020 conference. He is a technical consultant on the design and synthesis of RF and microwave passive filter and other components for 5G applications and beyond. He is currently working on the design, simulation and fabrication of the RF & microwave narrow band and broadband circulators. He now works for FILPAL (M) Sdn Bhd as the Technical Director. His role includes leading the training division in the company.

Socheatra SOEUNG was born in Phnom Penh, Cambodia, in 1986. He received his B.Eng. (Honors) degree in Electrical and Electronic, majoring in Computer System Architecture in 2010 from Universiti Teknologi PETRONAS, Malaysia. He completed his M.Sc. and Ph.D. degrees by research in Electrical and Electronics Engineering from Universiti Teknologi PETRONAS, Malaysia in 2013 and 2018, respectively. From 2014 to 2018, he worked as a research officer in RF Microwave Engineering under several Ministry of Higher Education Malaysia and industrial funding projects, while doing his Ph.D. degree. He was involved in designing, implementing, and testing RF subsystem components and RF links. Currently, he works as a lecturer and a computation and communication cluster leader at Universiti Teknologi PETRONAS in the Electrical and Electronic Engineering Department. He has been awarded several fundings as a project principle from the Malaysian Gov't, industries, and University research collaborations. His research interests include RF passive devices and circuits, filter design and synthesis, computer-aided tuning, and optimization techniques. He is currently an IEEE, MTT member, and committee member of IEEE ED/MTT/SSC Penang Chapter, Malaysia.